

Rainfall Contributions from Precipitation Systems with Different Sizes, Convective Intensities, and Durations over the Tropics and Subtropics

CHUNTAO LIU

Department of Atmospheric Sciences, University of Utah, Salt Lake City, Utah

(Manuscript received 27 May 2010, in final form 10 November 2010)

ABSTRACT

The rainfall contributions from precipitation features (PFs) with full spectra of different sizes and convective intensities over the tropics and subtropics are summarized using 12 yr of version 6 Tropical Rainfall Measuring Mission (TRMM) Precipitation Radar (PR) and Microwave Imager (TMI) observations. Regional, seasonal, and diurnal variations of the rainfall contributions from various PFs are shown, with the global distribution of the sizes, PR echo tops, maximum heights of 30 dBZ, and minimum TMI 85-GHz brightness temperatures of PFs above which contribute half of the rainfall in each $2^\circ \times 2^\circ$ region. Though the results from radar and microwave observations generally agree with each other, some large differences exist over land. Seasonal variations of sizes and intensities of precipitation systems are found over the northeast Pacific, northern SPCZ, and some land areas in addition to the well-known monsoon regions. The diurnal cycles of rainfall over land and ocean are interpreted with the combinations of life cycles of various precipitation systems, using the diurnal variations of rainfall contributions from precipitation systems with different sizes and intensities. The long-duration rainfall events with more than four consecutive 3-h periods with rain at a grid point are identified from 11 yr of TRMM 3B42 products. These “12-h rain events” contribute a larger proportion of the total rainfall over ocean than over land. They are mostly correlated with precipitation systems with large sizes and intense convection. However, they can also be caused by some shallow persistent precipitation systems, such as those over the northeast slope of the Andes in Peru in spring and fall and over the west coast of India in summer.

1. Introduction

As one of major components in the water cycle and closely related to our daily life, precipitation has been a focus of study and observation since early human history. However, only in recent decades have rain observations become near-globally available thanks to the technologies of space-borne passive microwave radiometers and radar (Wilheit 1986; Kummerow et al. 1998; Iguchi et al. 2000). The major advantage of space-borne radar and microwave radiometers is that they provide precipitation estimates over a large area with global coverage instead of “point” observations at specific locations by traditional rain gauges. With this advantage, the precipitation systems bringing the rainfall can be described over areas with few rain gauges, such as mountains, jungles,

and oceans. Furthermore, total amount of local rainfall may be apportioned into contributions from various precipitation systems globally.

There has been a long history of studying precipitation systems using satellite observations (Arkin et al. 1994; Adler et al. 2000; Huffman et al. 2001; Joyce et al. 2004). More recently, an algorithm has been developed using a contiguity test to group the area of a precipitation system and summarize its size, rain volume, and intensity using measurements from the space-borne radar and microwave radiometers (Mohr and Zipser 1996; Nesbitt et al. 2000; Toracinta and Zipser 2001; Toracinta et al. 2002). Applying this algorithm to the Special Sensor Microwave Imager (SSM/I; Spencer et al. 1989) and Tropical Rainfall Measuring Mission (TRMM; Kummerow et al. 1998) Precipitation Radar (PR) and TRMM Microwave Imager (TMI) observations, the global distribution of various precipitation systems have been studied, including mesoscale convective systems (Mohr and Zipser 1996; Mohr et al. 1999; Toracinta and Zipser 2001), extremely intense convective storms (Zipser et al. 2006), tropical

Corresponding author address: Dr. Chuntao Liu, Department of Atmospheric Sciences, University of Utah, 135S 1460E, Rm. 819, Salt Lake City, UT 84112-0110.
E-mail: liu.c.t@utah.edu

cyclones (Cecil et al. 2002; Jiang and Zipser 2010), deep convection penetrating the tropical tropopause (Liu and Zipser 2005), warm rainfall (Liu and Zipser 2009), and precipitation systems with lightning (Cecil et al. 2005; Liu et al. 2010). The rainfall contributions from these specific precipitation systems have been discussed. However, there has been no study providing a global view of rainfall contributions from precipitation systems with full spectra of different sizes and convective intensities partially due to the limited amount of observations. Now 12 yr of TRMM observations in 1998–2009 provide enough samples to do this.

Besides the rainfall intensity, the duration of the rainfall is one of the major factors controlling regional floods (Goel et al. 2000; Cunderlik and Ouarda 2007). Though the observations from nongeostationary satellites, such as SSM/I and TRMM, can only show “snapshots” of precipitation systems, the multisatellite products (e.g., Huffman et al. 2001) may provide the histories of precipitation systems with a 3-hourly interval. This 3-hourly temporal resolution is not fine enough to address the life cycles of some flash flood-related short-duration heavy rainfall events. But it is useful to describe the events lasting longer than 12 h and their contributions to the total rainfall locally (e.g., Skok et al. 2009).

Using 12 yr of TRMM PR and TMI observations, this study addresses the following questions:

- How much rainfall is contributed by precipitation systems with different sizes and convective intensities globally? What are the seasonal and diurnal differences of these rainfall contributions?
- How often do long-duration rainfall events occur over different regions? How much rainfall is contributed by these long-duration rainfall events globally? Are there any regional and seasonal differences?

Since rainfall estimates can be obtained from TRMM PR and TMI independently, the rainfall contributions from different precipitation systems are analyzed separately from PR and TMI observations. First, using the precipitation feature (PF) database containing characteristics of more than 120 million precipitation systems observed by TRMM from January 1998 to December 2009 (Liu et al. 2008), the spectra of rainfall contributions from PFs with different sizes, intensity proxies of maximum PR echo tops (Awaka et al. 1998), maximum height of PR 30-dBZ reflectivity, and minimum TMI 85-GHz polarization-corrected brightness temperatures (PCT; Spencer et al. 1989) are analyzed globally. Then the seasonal and diurnal variations of the sizes and intensities thresholds of PFs contributing 50% of rainfall are shown geographically. To demonstrate the importance of the rainfall events with long durations, the events with more

than four consecutive 3-h periods with rain at a $0.25^\circ \times 0.25^\circ$ grid point are identified from 11 yr of TRMM 3B42 product (Huffman et al. 2007). The geographical distributions of rainfall contributions from these long-duration rainfall events are shown seasonally.

2. Data and methods

The PFs used in this study are from the University of Utah TRMM PF database. A PF is defined by grouping the contiguous pixels with nonzero surface rain either from TRMM PR 2A25 products (Iguchi et al. 2000) called radar precipitation features (RPFs), or from TRMM TMI 2A12 products (Kummerow et al. 2001) called TMI precipitation features (TPFs). Then the characteristics of each RPF and TPF are summarized from collocated measurements and retrievals from the PR and TMI (see details in Liu et al. 2008). The properties of PFs used in this study include the following:

- Size—calculated from the number of PR pixels with nonzero 2A25 near-surface rain for RPFs and from the number of TMI pixels with nonzero 2A12 surface rain for TPFs;
- Volumetric rain—calculated from 2A25 near-surface rain for RPFs and from 2A12 surface rain for TPFs;
- Maximum detectable echo top (~ 18 dBZ; Yamamoto et al. 2008)—defined as the maximum storm height from the TRMM 2A23 products (Awaka et al. 1998) and the maximum height of a 30-dBZ echo from the PR;
- Minimum TMI 85-GHz PCT.

Using a same spatial sampling volume, only observations within PR swaths are used for both RPFs and TPFs. More than 102 million RPFs and 20 million TPFs are defined over 35°S – 35°N from 12 yr of TRMM version 6 data. There are more RPFs than TPFs for a few reasons. Because TMI has a larger footprint than PR, some small RPFs close to each other and distinguishable by PR may be grouped as one TPF by TMI. Sometimes a few RPFs embedded in thick anvil clouds could be grouped as one TPF because the TMI algorithm may show nonzero surface rainfall under these thick anvil clouds. Different sensitivities to the low rain rates from PR and TMI are another reason for the differences between RPFs and TPFs.

To calculate the rainfall contribution from various RPFs and TPFs, first RPFs and TPFs are categorized into bins of different sizes with lognormal intervals, different maximum echo-top heights with 0.25-km intervals, different maximum 30-dBZ heights with 0.25-km intervals, and different minimum 85-GHz PCTs with 10-K intervals in $2^\circ \times 2^\circ$ boxes over 36°S – 36°N based on their

properties and geo-center locations. Then the volumetric rainfall from these RPFs and TPFs are summarized in each bin and each box. In this way, the percent of rainfall contribution from RPFs and TPFs with properties within each bin are easily calculated by dividing from the rain volume in the bin to the total rain volume from all bins. Cumulative distribution functions of rainfall contributions from RPFs and TPFs with different sizes and intensities are obtained from percent contributions from various bins in each $2^\circ \times 2^\circ$ box. Using these cumulative distribution functions, the values of size, echo top, maximum height of 30 dBZ, and minimum 85-GHz PCT above which RPFs and TPFs contribute 50% of rainfall in each $2^\circ \times 2^\circ$ box are calculated. Similar analyses are repeated for RPFs and TPFs in four different seasons [i.e., December–February (DJF), March–May (MAM), June–August (JJA), and September–November (SON)] and six different local times (i.e., 0000–0400, 0400–0800, 0800–1200, 1200–1600, 1600–2000, and 2000–0000 LT) to present the seasonal and diurnal variations.

Usually with a larger size and more intense convection, a precipitation system tends to have a longer lifetime. The ideal way to demonstrate the life span of a precipitation system is to use an object-based method following the system's motion (e.g., Skok et al. 2009). But it is also important to demonstrate the continuous rainfall at any local points, which directly relate to the local flooding events. These local rain events are highly related to the lifetimes and the trajectories of the precipitation systems passing by. In this study, quasi-continuous rain events with more than four consecutive 3-h periods with rain at a grid point are identified from 11 yr of TRMM 3B42 products. The TMPA version of this product is used (Huffman et al. 2007), temporally grouped by using continuity test of nonzero 3-hourly rainfall data on each $0.25^\circ \times 0.25^\circ$ grid point. The duration and total rain amount for the events lasting longer than 12 h are summarized. Then their contributions to the total 3B42 rainfall on each $0.25^\circ \times 0.25^\circ$ grid are calculated.

3. Results

Mean annual rainfall over TRMM PR observation area (35°S – 35°N), tropics (20°S – 20°N), and subtropics (35° – 20°S and 35° – 20°N) from 12 yr of monthly TRMM PR (3A25) and TMI (3A12) retrievals are listed in Table 1. The mean annual rainfalls from PR and TMI agree with each other in general. There is a better agreement over ocean than over land. One reason for this land versus ocean difference is because TMI 2A12 uses different rainfall retrieval algorithms over land and over ocean because of the complex surface emissivity from land.

TABLE 1. 1998–2009 mean annual rainfall over the tropics and subtropics from TRMM PR (3A25) and TMI (3A12).

Annual rainfall (mm yr $^{-1}$)	Land and ocean	Land	Ocean
35°S–35°N PR	936	873	960
35°S–35°N TMI	991	1056	966
20°S–20°N PR	1160	1204	1145
20°S–20°N TMI	1229	1455	1153
35°–20°S and 35°–20°N PR	638	514	693
35°–20°S and 35°–20°N TMI	674	623	697

a. Rainfall contribution from PFs with different sizes and intensity

Multiplying the percent rainfall contributions from RPFs and TPFs categorized into the bins of different sizes to the mean annual rainfall, the rainfall contributions from RPFs and TPFs with different sizes are calculated over land and ocean in the tropics and subtropics separately and shown in Fig. 1. TPFs and RPFs both show that a larger proportion of rainfall comes from large systems over ocean than over land (blue curves shift to the right of red curves). This is consistent with the results of domination of rainfall contributions from mesoscale convective systems (MCSs) over these regions by Mohr et al. (1999) and Nesbitt et al. (2006). TPFs show larger land versus ocean differences in the rainfall contribution from different sizes than RPFs mainly because TMI 2A12 uses different rain detection algorithms over land and ocean. Especially over ocean, TPFs with area larger than $8 \times 10^4 \text{ km}^2$ contribute a relatively large proportion of rainfall compared with smaller contributions from RPFs and TPFs over land with similar sizes. Because TMI 2A12 uses observations at lower-frequency channels with larger footprints (Kummerow et al. 1998) for rainfall retrieval over ocean, the large footprint of the observations likely leads to larger TPF sizes because of small features being spread out over a larger footprint, and connecting small features that are in reality not contiguous. It is worth pointing out that RPFs with small sizes ($< 200 \text{ km}^2$) contribute more rainfall over ocean than those over land. Most of these small features are warm rain systems (Schumacher and Houze 2003; Liu and Zipser 2009). Note that the rain contribution from large systems ($> 30\,000 \text{ km}^2$) could be underestimated because of the PR swath width limit (Nesbitt et al. 2006).

Multiplying the percent rainfall contributions from bins of different echo tops and minimum 85-GHz PCTs to the mean annual rainfall, the rainfall contributions from RPFs and TPFs are similarly calculated over land and ocean in both tropics and subtropics and shown in Fig. 2. Over both latitude belts, TPFs and RPFs both

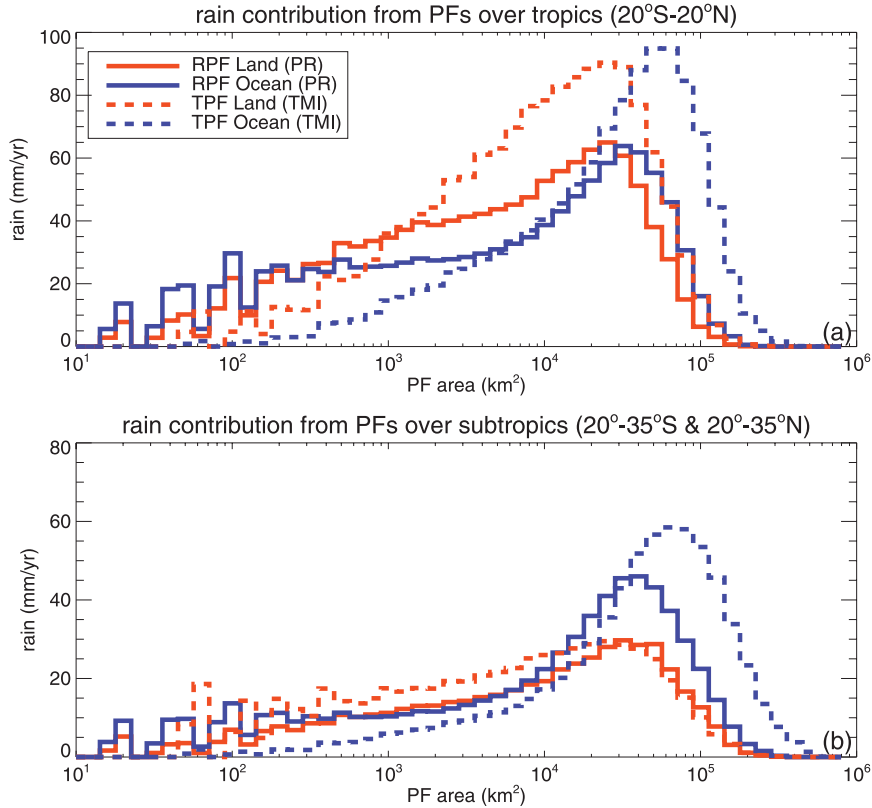


FIG. 1. Rainfall contributions from PFs defined using PR (RPFs, solid lines) and TMI (TPFs, dashed lines) rainfall retrievals with different sizes over the (a) tropics and (b) subtropics. The contributions are summarized over land (red lines) and ocean (blue lines) separately. Note that the total amount of rainfall under each curve adds up to the numbers listed in Table 1.

show that a larger proportion of rainfall is from more intense systems with high maximum echo tops and low minimum 85-GHz PCTs over land than those over ocean (red curves shift to the right of blue curves in Figs. 2a,b and to the left of blue curves in Figs. 2c,d). This is consistent with more intense convection over land in previous studies (e.g., Orville and Henderson 1986; Zipser et al. 2006). Figure 2a show that there are two peaks of rainfall contributions from PFs over ocean with echo top around 3 and 14 km. Two similar peaks of rainfall contributions are also shown for PFs over ocean with minimum 85-GHz PCT around 270 and 160 K over in Fig. 2c. These peaks represent the warm rain systems and deep convective systems over tropical oceans. Over the tropics, PFs with echo top >12 km contribute a large proportion of rainfall over both land and ocean. However, over the subtropics, the systems with echo top around 7–8 km contribute more than those with convection deeper than 12 km. The only exception is from TPFs over land (Fig. 2b) probably because version 6 TMI 2A12 may overestimate rainfall from deep convective systems with large thick anvil clouds over subtropical land (Wang et al. 2009).

Both Figs. 1 and 2 show that there are differences between rainfall contributions of various PFs from precipitation radar (RPFs, solid lines) and that from microwave radiometer (TPFs, dashed lines). These differences may be interpreted as resulting from different rainfall retrieval algorithms of the PR (Iguchi et al. 2000), microwave radiometers over land and ocean (Kummerow et al. 2001), different instrument footprints (Kummerow et al. 1998), different minimum detectable rain rate (Berg et al. 2006), and some collocation errors (Liu et al. 2008). The rainfall retrieval algorithms from PR and TMI also have different biases that could influence the rainfall contribution spectrums, such as underestimation of the warm rain over land by TMI (Wang et al. 2009) and overestimation of rainfall over the East China Sea by TMI because of the effects of aerosols (Berg et al. 2008). These differences in the rainfall retrieval between radar and microwave radiometer algorithms are not discussed further here, although they are the focus of work in progress (Nesbitt et al. 2004; Berg et al. 2006; Seo et al. 2007).

Figure 3 shows the geographical distributions of the sizes, highest PR echo tops, maximum height of 30-dBZ

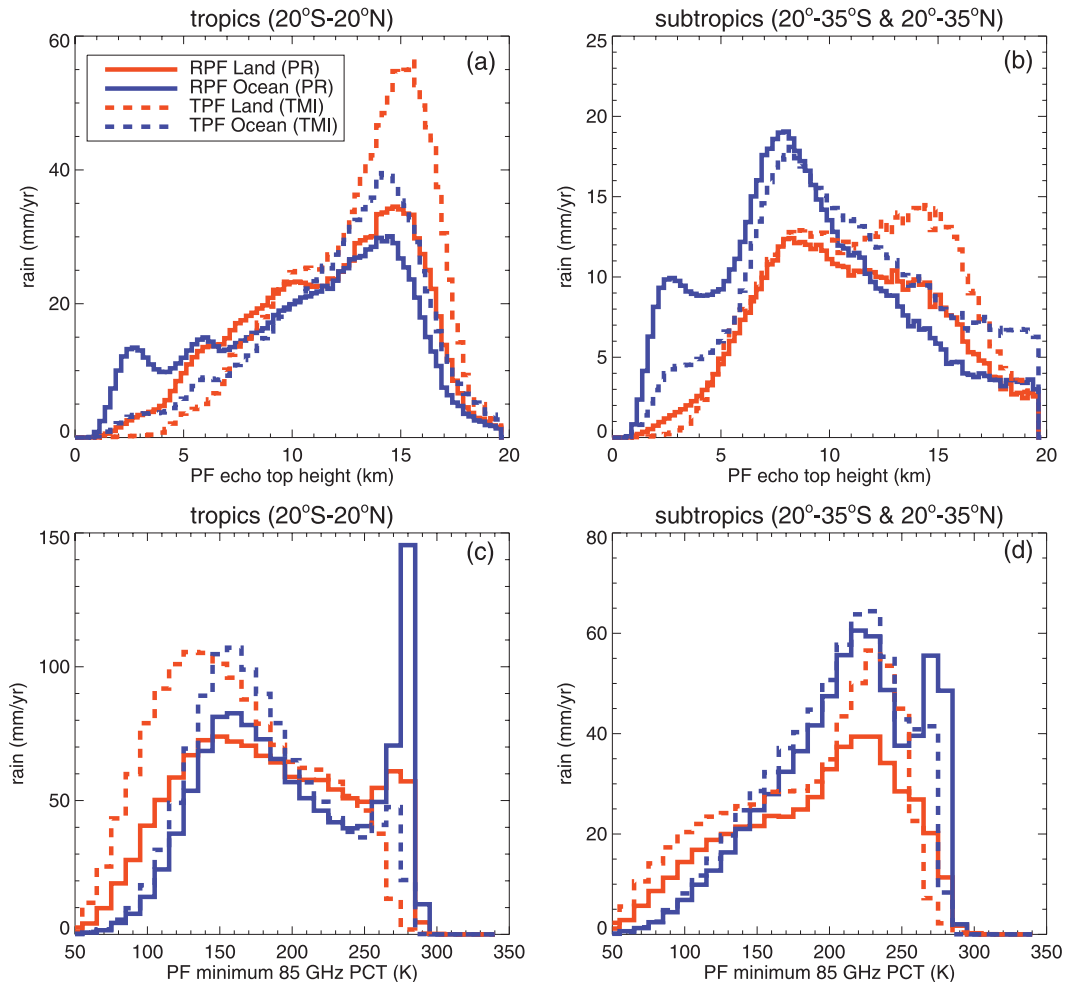


FIG. 2. As in Fig. 1, but for PFs with different (a),(b) maximum PR echo-top height and (c),(d) minimum TMI 85-GHz PCT. Note that the total amount of rainfall under each curve adds up to the numbers listed in Table 1.

echo, above which, and minimum 85-GHz PCT, below which RPFs contribute 50% of rainfall in $2^\circ \times 2^\circ$ boxes. In general, RPFs over subtropical oceans contributing 50% of local rainfall are larger than those in the ITCZ over tropical oceans (Fig. 3a). It is well known that extratropical cyclones are larger than their tropical counterparts and thus contribute relatively more rain in the subtropics. Large RPFs during the monsoon season over Argentina, southeast United States, and southeast China contribute a larger fraction of the local rainfall than the RPFs with similar sizes over the Amazon and central Africa (Fig. 3a). Tall systems with echo top reaching higher altitudes contribute most of the local rainfall over central Africa, Argentina, the north coast of Australia, the east coast of India, the west coast of Mexico, some parts of the Maritime Continent, and over the South China Sea (Fig. 3b). Except for these regions, there are no substantial differences between land and

ocean in the echo tops of RPFs contributing 50% local rainfall (Fig. 3b). However, the maximum heights of 30 dBZ of RPFs contributing half of the local rainfall are relatively higher over land than those over ocean (Fig. 3c). The minimum 85-GHz PCTs of RPFs contributing half of the local rainfall are relatively lower over land than those over ocean (Fig. 3d). These are consistent with earlier studies that show stronger convection over land than over ocean (Mohr and Zipser 1996; Nesbitt et al. 2000; Zipser et al. 2006). With a stronger updraft, large size ice particles such as graupels or hails may reach higher altitude and have a higher radar reflectivity and a stronger ice scattering signal in microwave brightness temperatures in convection over land than that over ocean. However, the maximum heights of precipitation systems over land and ocean can be close to each other because of the small differences in their levels of neutral buoyancy (Liu et al. 2007). Analyses of TPFs show similar

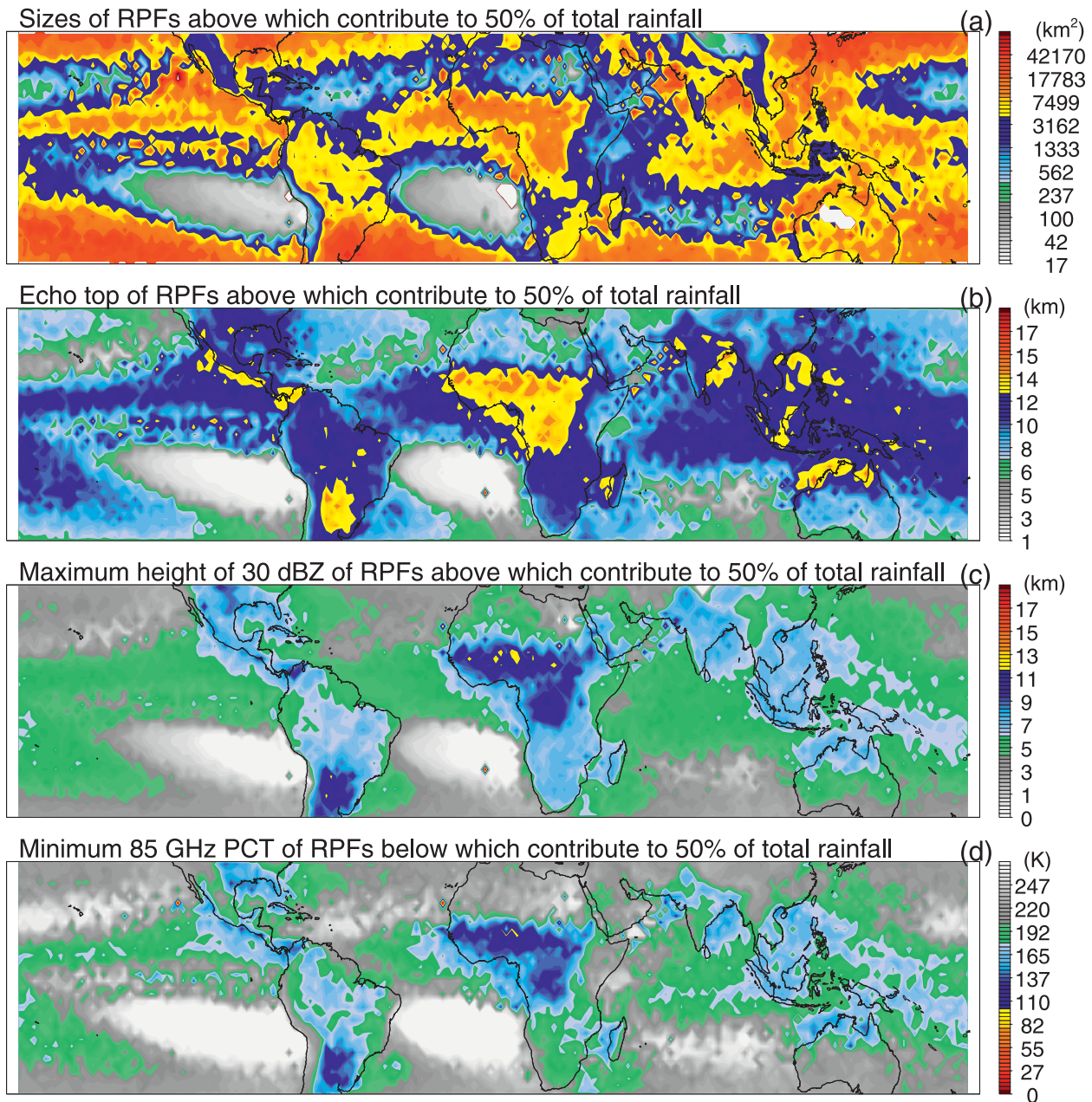


FIG. 3. Global distribution of properties of RPFs contributing to 50% of the local rainfall. (a) RPFs with sizes above which contribute 50% of the local rainfall, (b) maximum PR echo-top height, (c) maximum height of 30 dBZ, and (d) minimum TMI 85-GHz PCT.

geographical patterns as that of RPFs in Fig. 3, but with larger sizes and more land versus ocean contrasts due to the different algorithms (not shown).

b. Seasonal variation

It is obvious that precipitation systems over various regions have different properties in different seasons. Figure 4 shows the geographical distributions of the sizes of RPFs contributing half of local rainfall in four different

seasons. Over all, as in Fig. 3a, large subtropical systems contribute more rainfall locally than tropical systems. Oceanic systems in general are larger than land systems, but there are some large MCSs during the monsoon season over Argentina, the southeast United States, and Southeast Asia. These are consistent with earlier results on the MCS studies (Houze and Churchill 1987; Mohr and Zipser 1996; Nesbitt et al. 2000). Besides the known seasonal variations of the MCSs over monsoon regions,

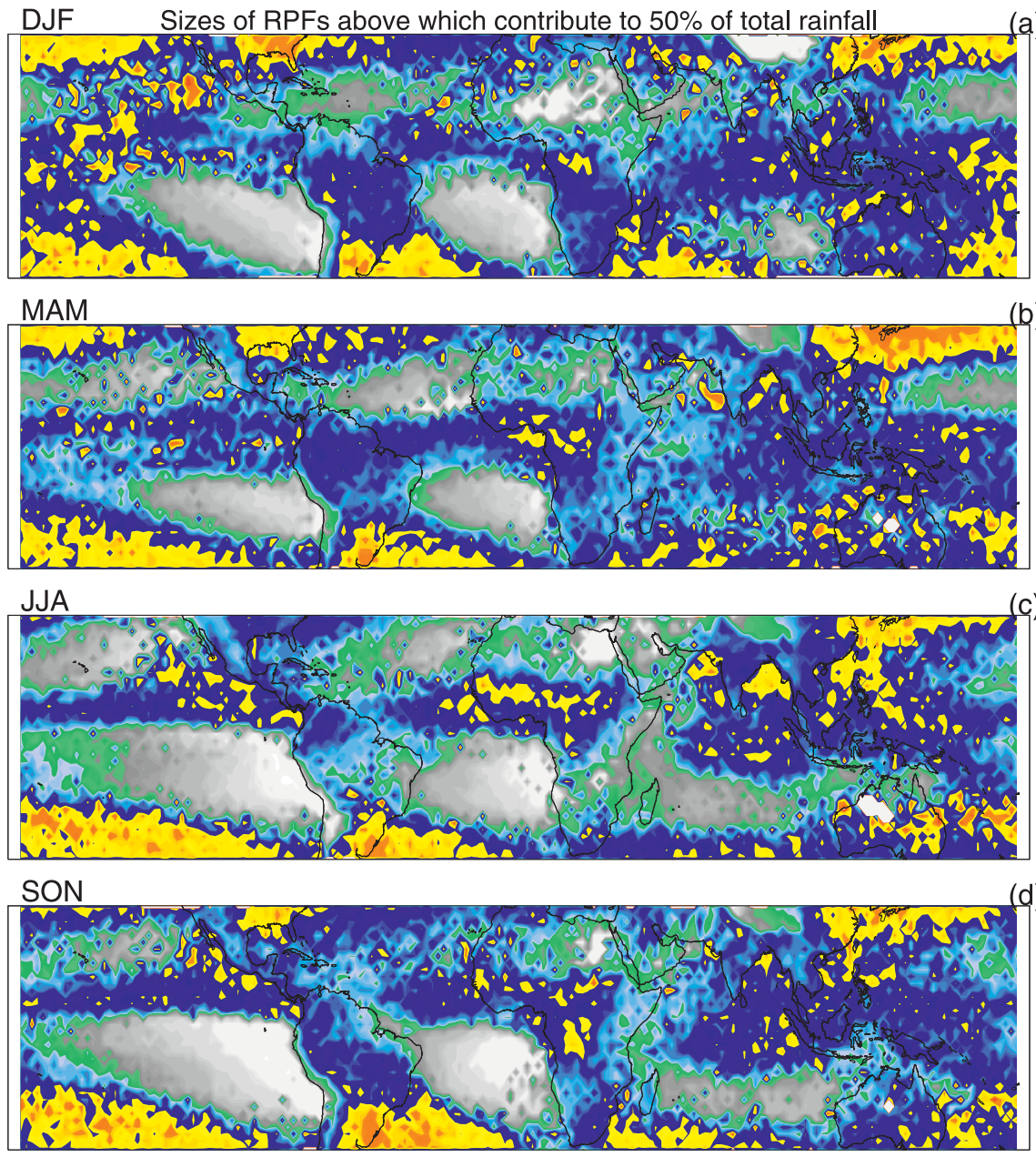


FIG. 4. Global distribution of sizes of RPFs above which contribute to 50% of the local rainfall in different seasons (DJF, MAM, JJA, and SON).

there are some interesting features in Fig. 4. For example, though there is not much rainfall over the east Pacific north of the ITCZ in DJF, most of the rainfall over the region is from a few large precipitation systems (Fig. 4a). Precipitation systems over the east Pacific ITCZ are larger in JJA and SON than in DJF and MAM. Some of them may persistent more than 2 days (Figs. 13c,d). Similar large and long-lasting precipitation systems are also found over the northern SPCZ in DJF

(Figs. 4a and 13a). It is also interesting to see the changing sizes of small warm rainfall systems in the southeast Pacific that are related to the large-scale descent over the region. Small systems in JJA contribute a larger proportion of rainfall over many land regions including the Amazon, South Africa, the southeast United States, and southeast China than in other seasons. This is due to the dominated small systems in the dry season of the Amazon and South Africa, and the more isolated thunderstorms

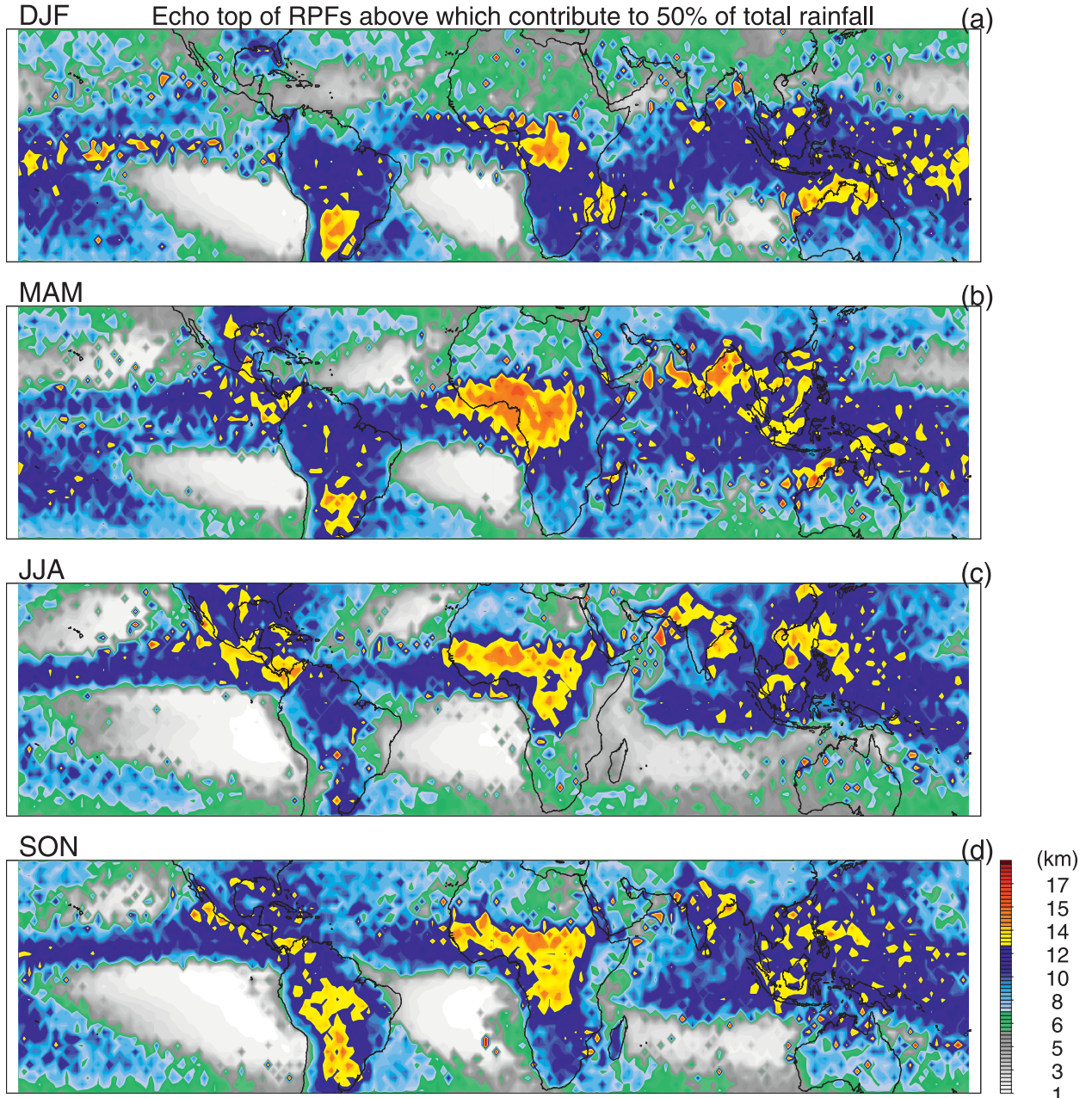


FIG. 5. As in Fig. 4, but for echo tops of RPFs.

rather than the organized MCSs over the southeast United States and China in JJA.

The geographical distributions of the maximum echo tops of RPFs contributing half of local rainfall in four different seasons are shown in Fig. 5. There is a clear shift of regions for large contribution from tall systems, from the Bay of Bengal in MAM to northern India along the south slope of the Himalayas in JJA as pointed out by Houze et al. (2007). Though significant amount of rainfall is observed over the western coast of India in JJA,

the precipitation systems are relatively shallow (Figs. 5c and 7). In DJF, precipitation systems with higher echo tops (Fig. 5a) and lower minimum 85-GHz PCTs (figure not shown) contribute more rainfall over the Pacific ITCZ than those with similar properties in other seasons. Precipitation systems over the Amazon only become stronger with higher echo tops (Fig. 5d) and lower 85-GHz PCTs (not shown) in SON. Analyses of TPFs show similar seasonal variations of geographical patterns as that of RPFs in Figs. 4 and 5 (not shown).

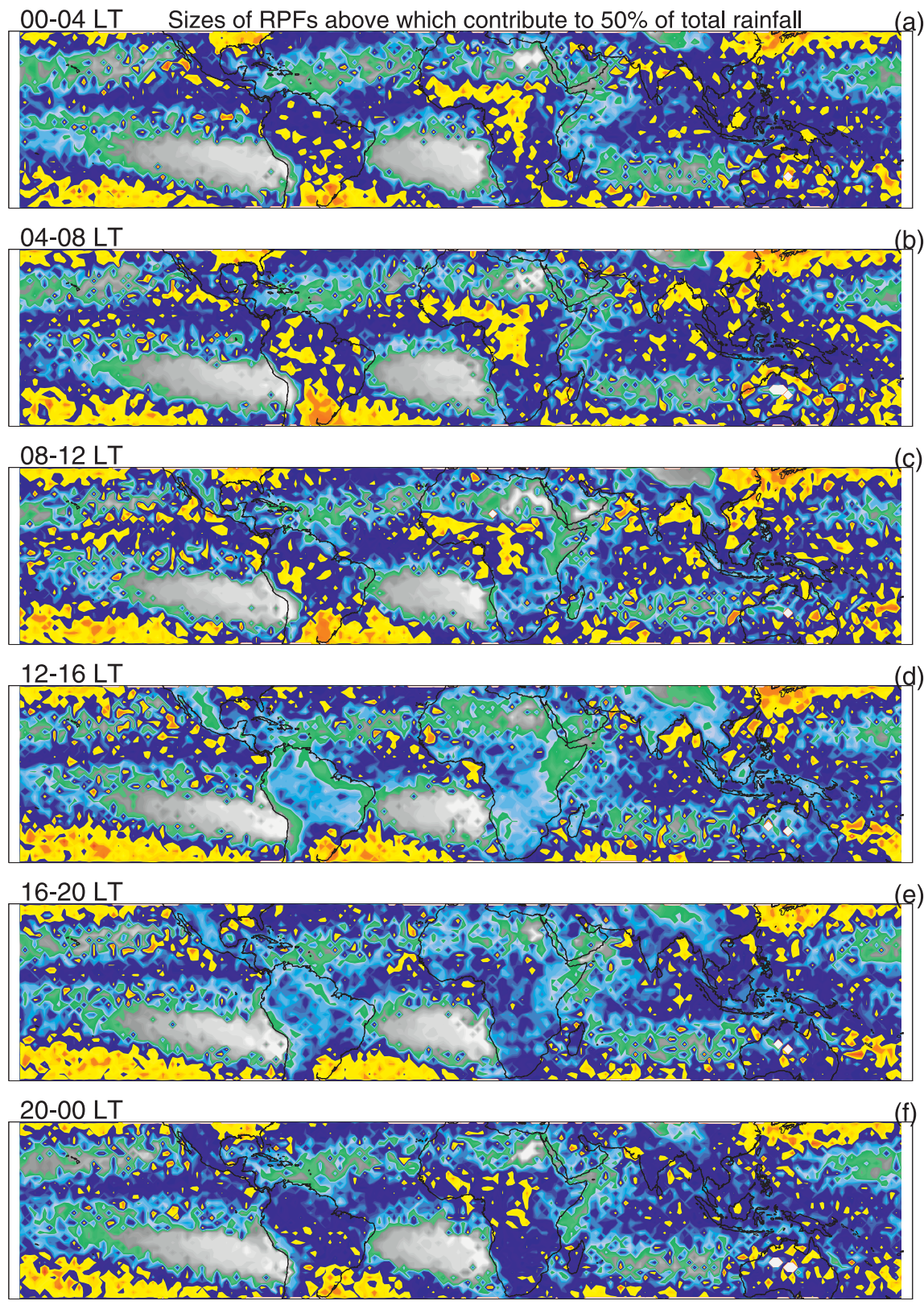


FIG. 6. As in Fig. 4, but for RPFs which contribute to 50% of the local rainfall during different local time periods.

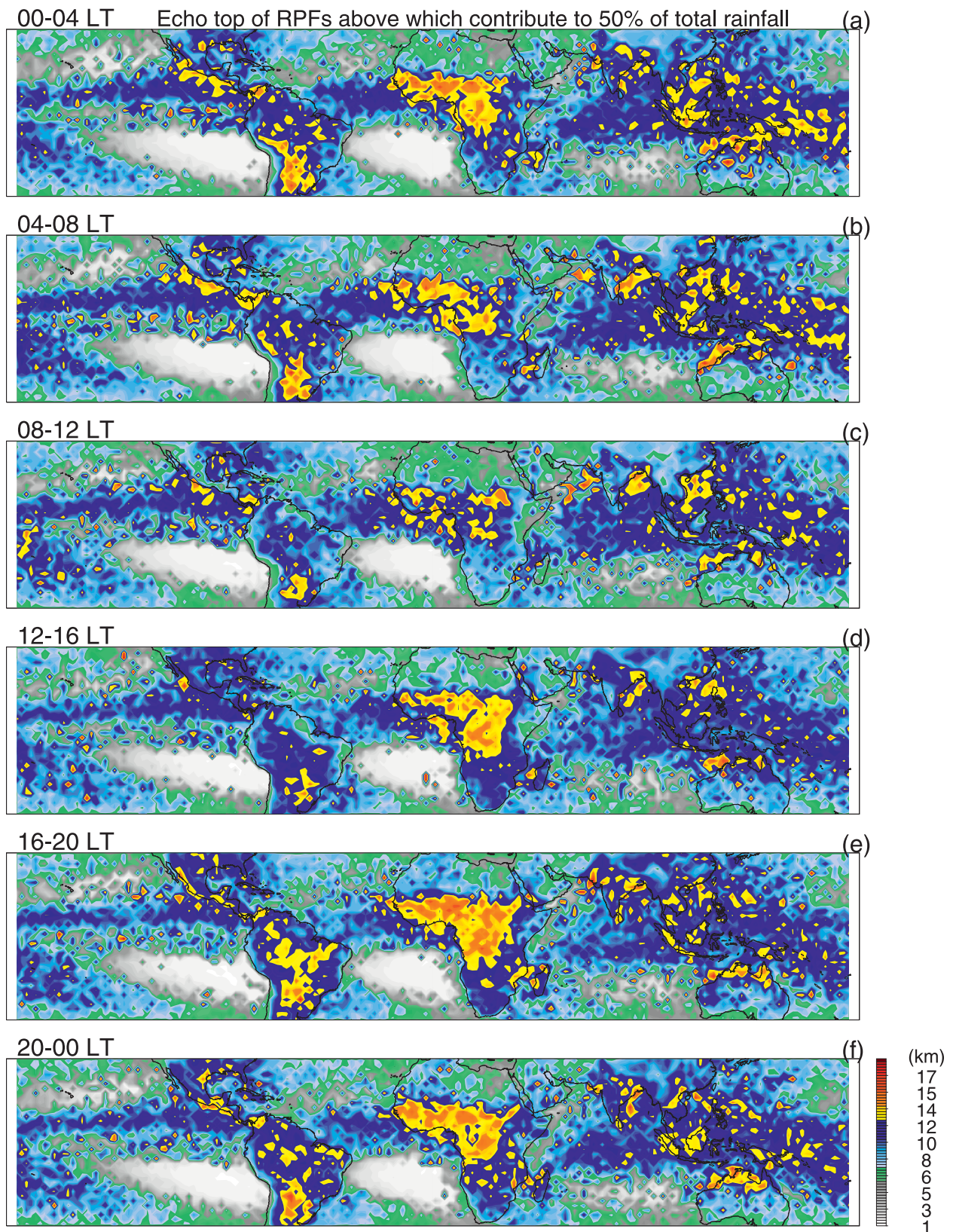


FIG. 7. As in Fig. 5, but for RPFs above which contribute to 50% of the local rainfall during different local time periods.

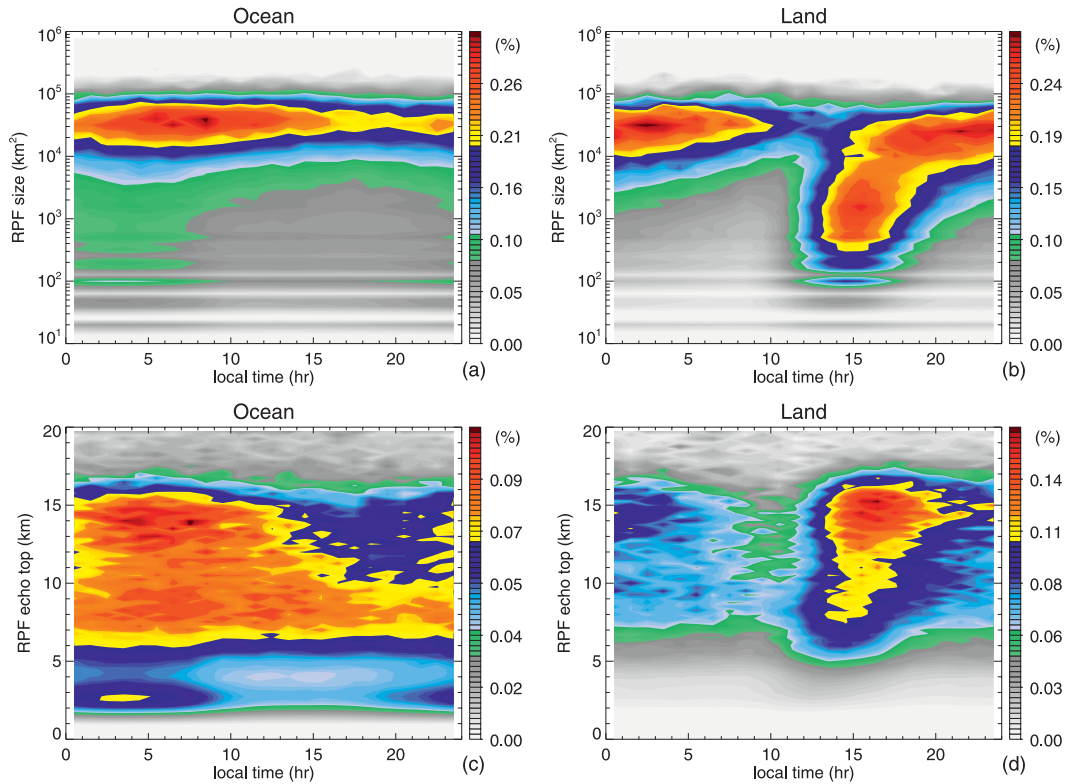


FIG. 8. Diurnal variations of rainfall contribution from RPFs with (a),(b) different sizes and (c),(d) echo tops over 35°S–35°N for (left) land and (right) ocean. The local times are divided into 24 1-h bins. Sizes are divided into the same bins as in Fig. 1. Echo-top heights are divided into 80 bins with 250-m intervals. The values in each add up to 100%.

c. Diurnal variation

The geographical distributions of the sizes and maximum echo tops of RPFs contributing half of the local rainfall in six different local time periods are shown in Figs. 6 and 7. It is well known that there is a stronger diurnal variation of rainfall and convection over land than over ocean (Hall and Vonder Haar 1999; Yang and Slingo 2001; Nesbitt and Zipser 2003; Liu and Zipser 2008). This can be clearly seen with the contrast between the rainfall contributions from small precipitation systems in the early afternoon (Figs. 6d,e) and that from large precipitation systems in the evening and early morning (Figs. 6a,b) over the Amazon, central Africa, and India. Over some land regions, this early afternoon versus early morning contrast is not as significant, such as over the southeast United States and China. Consistent with the early afternoon development of convection over land, more rainfall is from deep precipitation systems over the Amazon and central Africa from afternoon to midnight, though the precipitation systems over Africa are taller than those over the Amazon (Figs. 7d–f). It is known that deep convection over both Argentina and the southeast United States are very intense (Zipser

et al. 2006). Some of the giant MCSs over Argentina may last longer and contribute a larger portion of rainfall during the early morning (Figs. 7a–c; Salio et al. 2007). Note that some deep precipitation systems develop over the east coast of India, the west coast of Mexico, and the northwest coast of Australia in the early morning (Fig. 7b) and contribute a large proportion of local rainfall.

To summarize the diurnal variations of the rainfall contributions from PFs with different sizes and intensities, the fractional rainfall contributions from all RPFs over 35°S–35°N land and ocean are shown with 24-h local time bins and different sizes, echo tops, maximum height of 30 dBZ, and from all TPFs with minimum 85-GHz PCT bins in Figs. 8 and 9. Over land, small and moderate precipitation systems dominate the rainfall contribution in the early afternoon while small systems contribute less from the evening to the following morning. This is consistent with the domination of the MCS in the early morning pointed out by Nesbitt and Zipser (2003). From Figs. 9b,d, strong convection in the precipitation systems with high 30-dBZ height diminishes from midnight (5–13 km) to early morning (5–8 km) over land. But the echo tops of these precipitation systems are still high (around 13–15 km) in the early morning

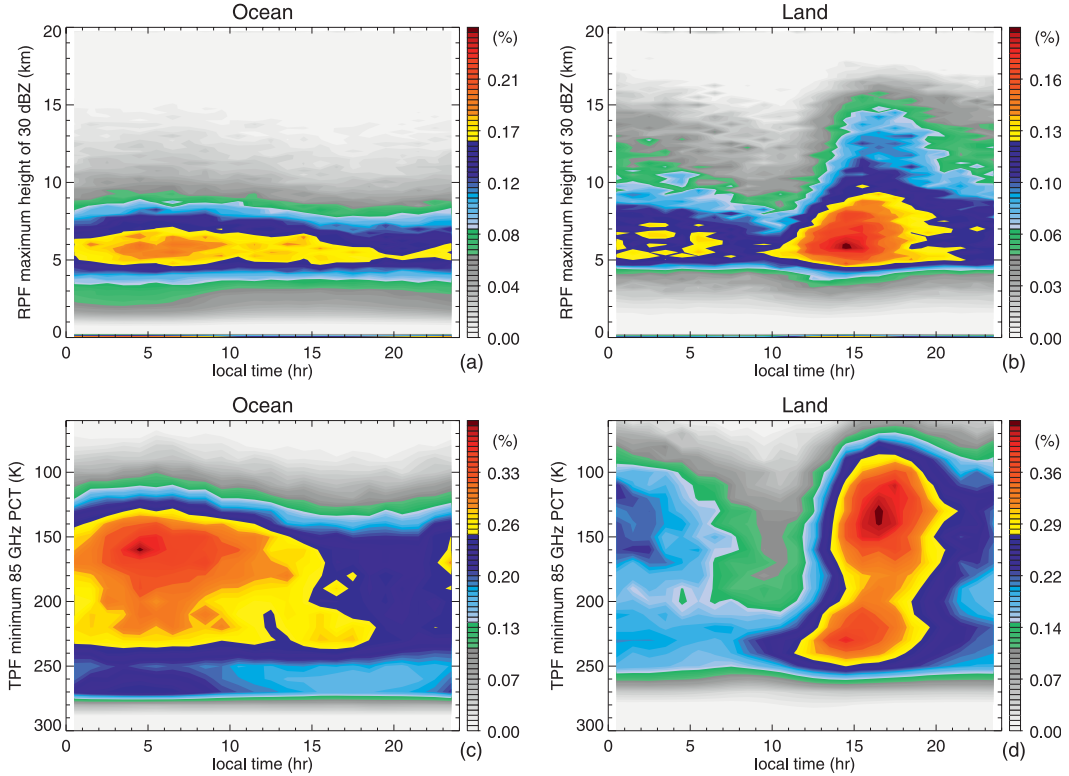


FIG. 9. As in Fig. 8, but from (a),(b) RPFs with different maximum heights of 30 dBZ and (c),(d) TPFS with minimum 85-GHz PCTs.

(Fig. 8d), as the convection and deep stratiform rain persists in these still-active MCSs for some time as they slowly weaken (e.g., Velasco and Fritsch 1987). Over the ocean, the diurnal variation of rainfall and convection has a smaller amplitude with a shallow rain peak in the early morning. Large precipitation systems dominate the rainfall contribution all the time (Fig. 8a). Deep precipitation systems with high echo tops have a greater contribution in the early morning, decreasing toward late afternoon. In the afternoon and evening, precipitation systems with echo tops below 10 km contribute most of the rainfall. Note that warm rain systems (echo top below 4 km with maxima around 0300–0400 LT) have a relatively stronger diurnal cycle with a maximum about 1–2 h earlier than the maximum of the deep systems (echo top above 12 km with maxima around 0400–0600 LT) in the early morning (Figs. 8c and 9c).

Further demonstrating the diurnal cycles of precipitation systems with different sizes and intensities, RPFs over land and ocean with sizes greater than 1000 km^2 contributing most of the total rainfall (Fig. 8a) are divided into four categories based on the median values of their sizes and maximum heights of 30 dBZ (Figs. 10a,c). The diurnal variations of the populations of the RPFs in each category are shown in Fig. 10. Over land, the

small systems with intense convection peak first in the early afternoon (1500–1700 LT). Some of them become larger, with intense convection, peak later within 2 h. The remainder becomes weaker. In the evening and early morning, the weak convection sustains the large systems until their dissipation (Fig. 10d). We speculate that the stratiform fraction of these MCSs is greatest in the early morning before dissipation. This is consistent with the diurnal variation of MCSs shown by Nesbitt and Zipser (2003). Over the ocean, the sequence of peaks of small and intense, large and intense, and large and weak systems is similar, but with a weaker diurnal cycle and peaks shortly before sunrise for intense systems (Fig. 10b). This is consistent with the life cycles of various precipitation systems. Analyses of TPFS show similar diurnal variations as that of RPFs (not shown).

d. Rainfall contribution from long-duration rain events

From 11 yr of the 3B42 product, about 6 million events with $\geq 12\text{-h}$ quasi-continuous rain on $0.25^\circ \times 0.25^\circ$ grids are identified per year. About 12% of them are found with $\geq 24\text{ h}$ quasi-continuous rainfall. The geographical distribution of the annual number of these events

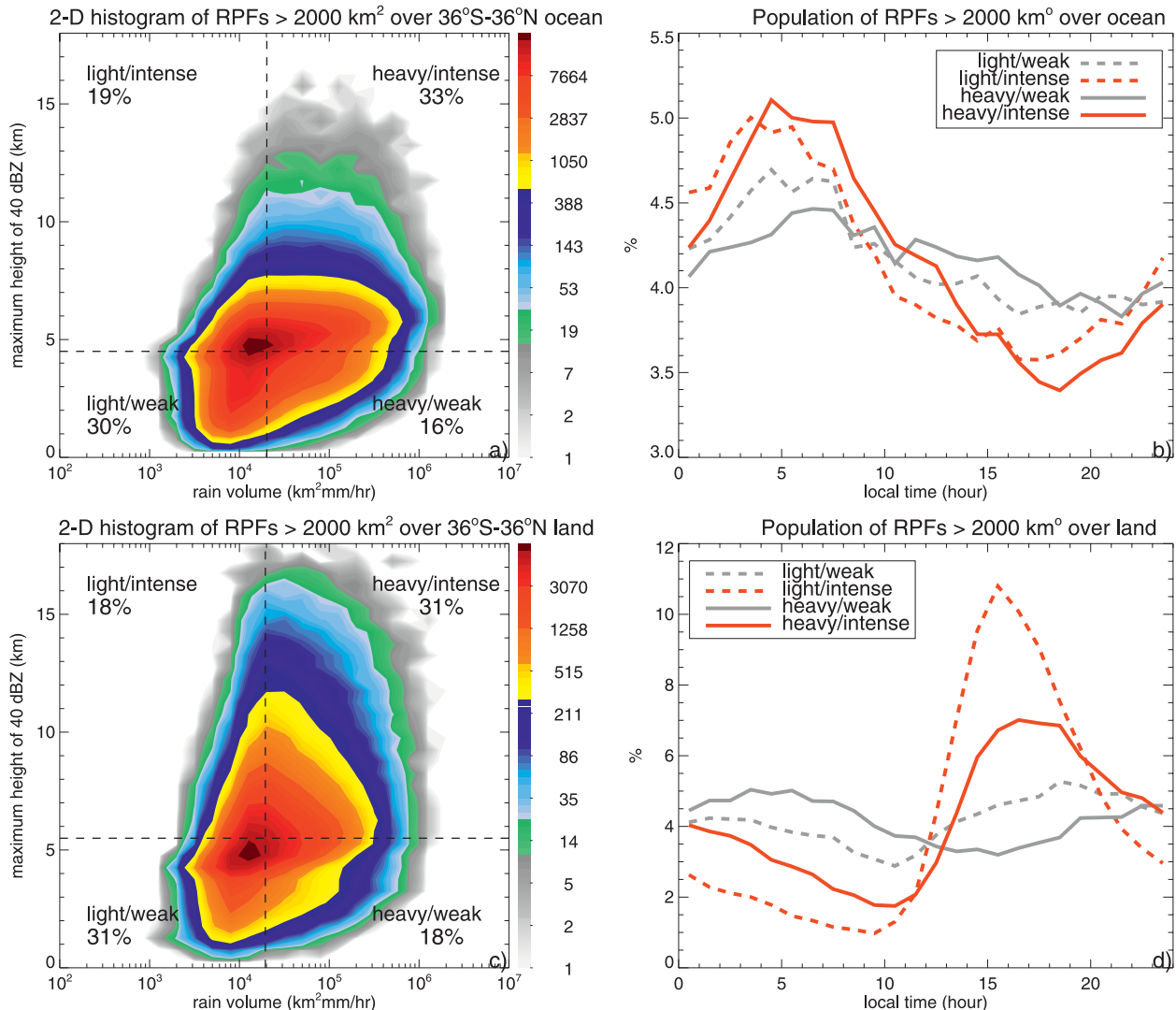


FIG. 10. (a) The 2D histogram of volumetric rainfall and maximum height of 40 dBZ of RPFs with size greater than 2000 km² over the ocean (36°S–36°N). The median value of volumetric rainfall and maximum height of 40 dBZ are shown with two dashed lines and divided the RPF samples into four categories of light rain with weak convection, light rain with intense convection, heavy rain with weak convection, and heavy rain with intense convection. (b) Diurnal variations of population of the four categories of RPFs in (a). (c) As in (a), but over land. (d) Diurnal variations of population of the four categories of RPFs in (c). Note the scale differences in (b) and (d); diurnal variation amplitude is much stronger over land than that over the ocean.

and their rainfall contributions are shown in Fig. 11. There are more long-duration rain events over ocean than over land (Figs. 11a,c). As discussed earlier, oceanic systems have relatively larger-sized and weaker diurnal cycles that help them last longer than land systems. Besides the strong diurnal cycle that prevents the long lifetime of land systems, land systems are often fast moving, which does not favor a long continuous local rainfall. The 24-h rainfall events are very rare over land, but relatively more frequent over the east Pacific ITCZ than any other region (Fig. 11c). The 12-h rain events contribute to more than half of the rainfall not only over

the ocean regions with large amounts of annual rainfall, such as ITCZ and SPCZ, but also over low-rainfall oceans such as the Arabian Sea and off the northwest coast of Australia (Fig. 11b). Many of the long-duration events over the Arabian Sea and off the northeast coast of Australia are over 24 h (Fig. 11d). A large portion of the rainfall over these regions is from tropical cyclones (Jiang and Zipser 2010). Most of the long-duration rain events over the East China Sea are due to the stationary fronts with a large contribution to the local rainfall during the mei-yu season (Chen 2004; Xu et al. 2009). Over Papua-New Guinea and Borneo, there are many

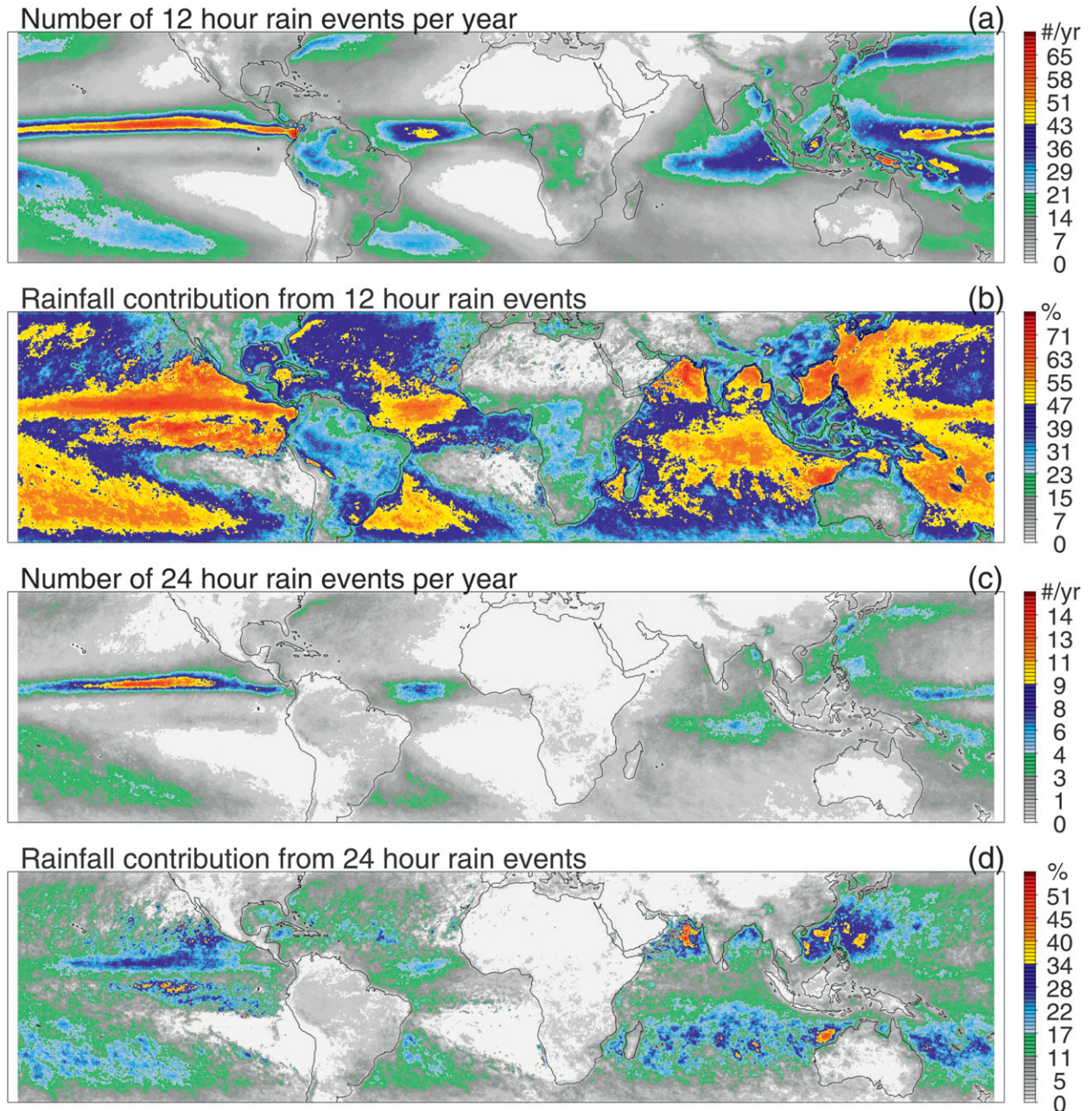


FIG. 11. (a) Global distribution of the numbers of events with 12-h continuous rain per year. The 12-h continuous rain events are defined using 3-hourly 3B42 product on $0.25^\circ \times 0.25^\circ$ grids. Note that we assume that each nonzero rainfall from 3B42 has 3-h continuous rain, which may not be correct all the time. (b) Total rainfall contribution from these 12-h continuous rain events. (c) Global distribution of the numbers of events with 24-h continuous rain per year. (d) Total rainfall contribution from those 24-h continuous rain events in (c).

12-h duration events, but relatively small rain contributions are from them. Probably this is because of the large number of small and short-duration events as pointed out by Skok et al. (2009). Note that because TRMM 3B42 products rely heavily on the rainfall retrievals from microwave observations, part of the land versus ocean contrast shown in Fig. 11 is probably due

to the different rain retrieval algorithms over land and ocean.

The seasonal variations of the rainfall contribution from long-duration events over land are shown in Fig. 12. Though long-duration rain events are relatively rare over land, they have significant contributions to the local rainfall over some regions in certain seasons, to name

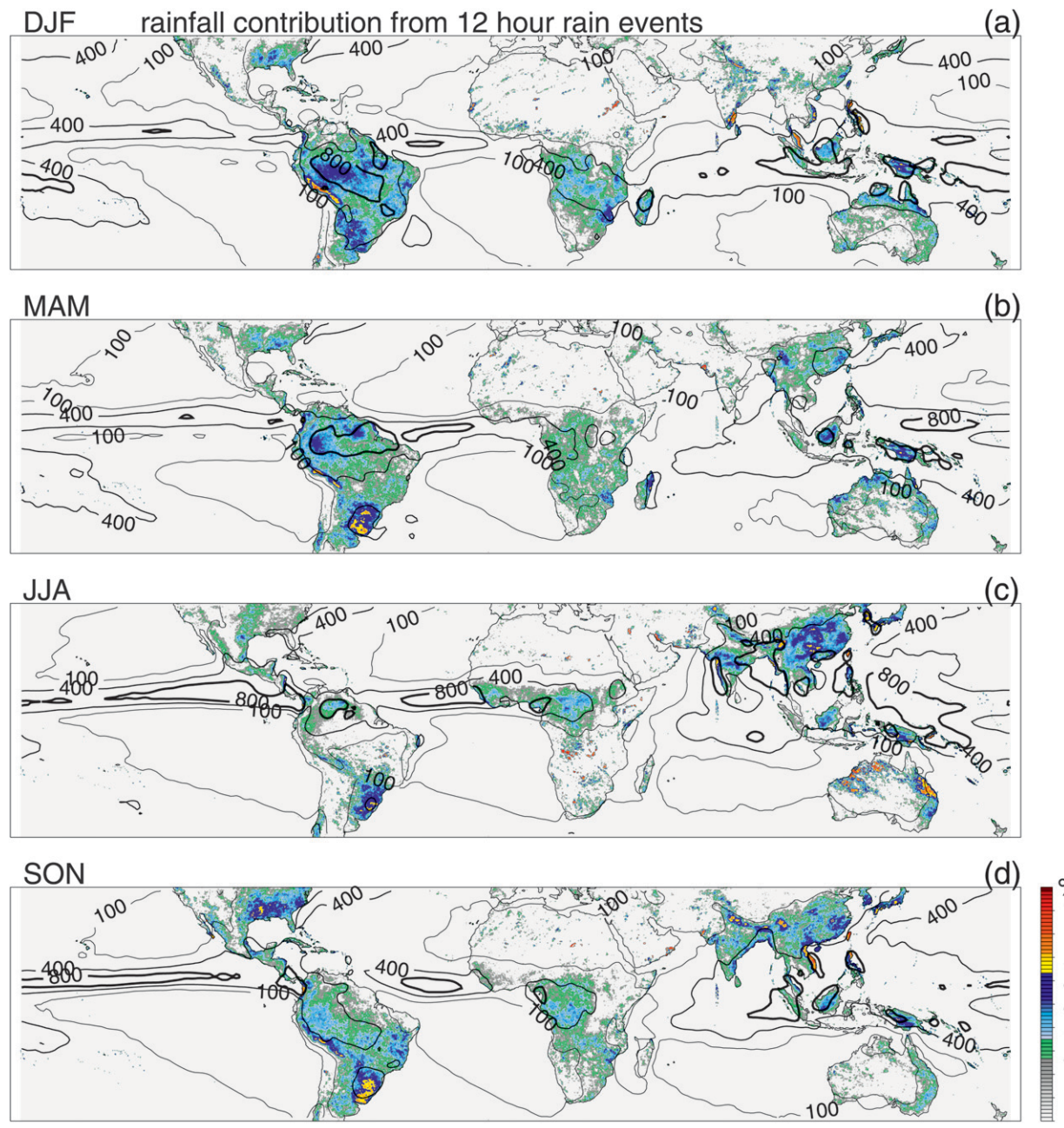


FIG. 12. Rainfall contribution from 12-h rain events over land in different seasons (color shading). Mean 3B42 seasonal rainfall amounts are contoured with 100, 400, and 800 mm season^{-1} . Note that there are some extremely high percentages of contributions from 12-h rain events over the desert regions, such as the Sahara, Kalahari, and Arabian. These are probably due to the rain detection problems over desert regions from microwave radiometers (Wang et al. 2009).

a few, the east coast of India, the northeast slope of the Andes, and Malaysia and Philippines in DJF, the northeast and northwest coasts of Australia in JJA, the east coast of Vietnam in SON, southeast China and the west coast of India in JJA, the northeast slope of the Andes in Peru, and over Argentina in most seasons. The causes of these long-duration events are diverse, including the impact

of terrain on the low-level jets (Falvey and Garreaud 2005), the quasi-stationary mei-yu front during the monsoon (Chen 2004), and large MCSs with long lifetimes (Salio et al. 2007).

The locations of the extreme long local rainfall events spanning more than 2 days are shown in Fig. 13. Over land, there are not many rain events longer than 2 days

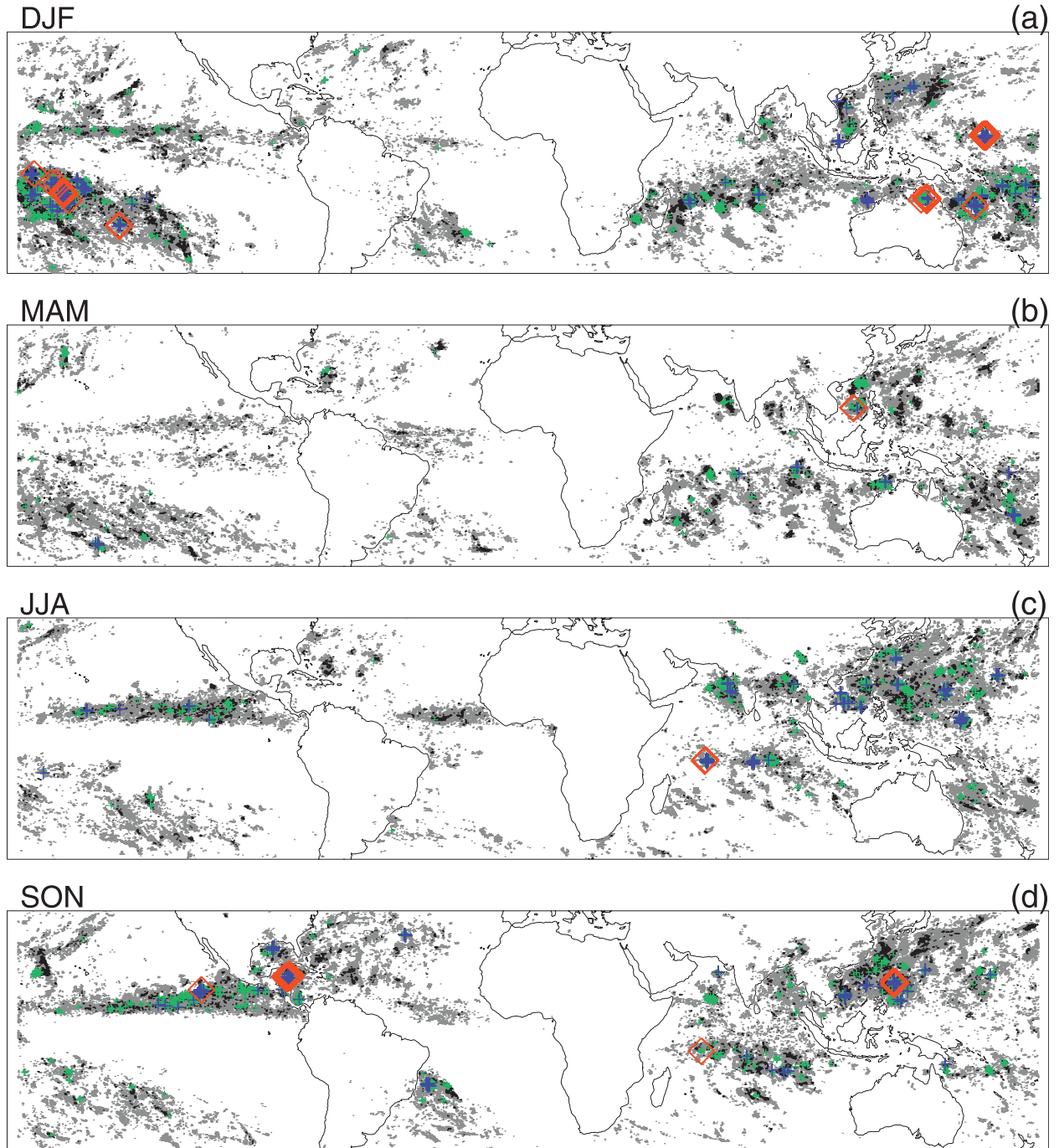


FIG. 13. Locations of extreme long rain events in different seasons. The gray dots, black dots, gray crosses, blue crosses, and red diamonds represent rain events longer than 2, 3, 4, 5, and 6 days during 1998–2008.

except some over India, Southeast Asia during the Asian monsoon in JJA, and some events over the Amazon in DJF. This may not be a fair comparison because TRMM TMPA products over land may underestimate the rain, especially the warm rain (Wang et al. 2009). Note that the shallow precipitation systems over the

west coast of India in JJA also tends to persist for a long time. Most of long rainfall events happen over the ocean, many of them are related to the tropical cyclones, such as over the northwest of the Atlantic and Pacific in SON. The long events over the east Pacific in JJA and SON and over the SPCZ in DJF are consistent with large

precipitation systems as shown in Fig. 4. Focused studies on these regions are required to interpret these events properly and are not discussed in detail here.

4. Conclusions

Using 12 yr of TRMM observations, the rainfall contributions from precipitation systems with different sizes and intensities are shown globally. The importance of long-duration rain events over different regions are shown with 12-h quasi-continuous rainfall events identified from the TRMM 3B42 product from 1998 to 2008. The following general results are consistent with earlier studies:

- Precipitation systems over land are more intense than those over ocean. However, a larger proportion of the total rainfall over ocean is contributed by precipitation systems that are shallower and weaker than those over land.
- Large precipitation systems contribute a larger proportion of rainfall over the subtropics than over the tropics in general. Over monsoon regions, there are large seasonal variations of sizes and intensities of precipitation systems that dominate the contribution of rainfall.
- The diurnal variations of the rainfall contribution can be interpreted in terms of the life cycle of convection, especially large MCSs over land. The diurnal variations of rainfall over ocean are relatively small, with weak night and early morning maxima for both large and small features.
- There are fewer rain events with over 12-h duration over land than over ocean, but long-duration rain events over some land regions are significant in certain seasons.

Besides these, some detailed relations between rainfall and precipitation systems have been revealed and quantified in this study:

- For the first time, contributions of global rainfall from precipitation systems with full spectra of different size and intensities are summarized using both radar and microwave observations. Though the results from radar and microwave observations generally agree with each other, some large differences exist, especially over subtropical land.
- Some interesting seasonal variations of sizes and intensities of precipitation systems are shown: a few large precipitation systems over the dry region to the north of ITCZ in the northeast Pacific contribute most of the local rainfall in DJF. In JJA, precipitation systems over the Amazon, South Africa, the United States, and southeast China have a relative smaller size than in other seasons; there are large seasonal

variations of sizes of precipitation systems over the east Pacific. This is very well correlated with the seasonal variations of the long-lasting rainfall events over the region.

- For the first time, the diurnal variations of rainfall contribution from precipitation systems with different size and intensity have been shown. With these variations, the diurnal cycles of rainfall over land and ocean are interpreted with the combinations of life cycles of various precipitation systems.
- Long-duration local rainfall events are shown mostly correlated with precipitation systems with large sizes and intense convection. However, they may also be from some shallow persistent precipitation systems, such as those over the northeast slope of the Andes in Peru in MAM and SON and over the west coast of India in JJA.

Acknowledgments. This research was supported by NASA Precipitation Measurement Mission Grants NAG5-13628 under the direction of Dr. Ramesh Kakar and NASA Grant NNX08AK28G under the direction of Dr. Erich Stocker. Special thanks go to Dr. Edward Zipser for his valuable comments and English editing. Thanks also go to Dr. Daniel Cecil and two anonymous reviewers for their valuable suggestions that improved the quality of this paper. Thanks to Drs. Erich Stocker and John Kwiatkowski and the rest of the TRMM Science Data and Information System (TDSIS) at NASA Goddard Space Flight Center, Greenbelt, MD, for data processing assistance.

REFERENCES

- Adler, R. F., G. J. Huffman, D. T. Bolvin, S. Curtis, and E. J. Nelkin, 2000: Tropical rainfall distributions determined using TRMM combined with other satellite and rain gauge information. *J. Appl. Meteor.*, **39**, 2007–2023.
- Arkin, P. A., R. J. Joyce, and J. E. Janowiak, 1994: IR techniques: GOES precipitation index. *Remote Sens. Rev.*, **11**, 107–124.
- Awaka, J., T. Iguchi, and K. Okamoto, 1998: Early results on rain type classification by the Tropical Rainfall Measuring Mission (TRMM) precipitation radar. *Proc. Eighth URSI Commission F Open Symp.*, Aveiro, Portugal, URSI, 143–146.
- Berg, W., T. L'Ecuyer, and C. Kummerow, 2006: Rainfall climate regimes: The relationship of regional regional TRMM rainfall biases to the environment. *J. Appl. Meteor. Climatol.*, **45**, 434–454.
- , —, and S. V. D. Heever, 2008: Evidence for the impact of aerosols on the onset and microphysical properties of rainfall from a combination of satellite observations and cloud-resolving model simulations. *J. Geophys. Res.*, **113**, D14S23, doi:10.1029/2007JD009649.
- Cecil, D. J., E. J. Zipser, and S. W. Nesbitt, 2002: Reflectivity, ice scattering, and lightning characteristics of hurricane eyewalls

- and rainbands. Part I: Quantitative description. *Mon. Wea. Rev.*, **130**, 769–784.
- , S. J. Goodman, D. J. Boccippio, E. J. Zipser, and S. W. Nesbitt, 2005: Three years of TRMM precipitation features. Part I: Radar, radiometric, and lightning characteristics. *Mon. Wea. Rev.*, **133**, 543–566.
- Chen, G. T.-J., 2004: Research on the phenomena of Meiyu during the past quarter century: An overview. *The East Asian Monsoon*, C.-P. Chang, Ed., World Scientific Publishing, 357–403.
- Cunderlik, J. M., and T. B. M. J. Ouarda, 2007: Regional flood-rainfall duration-frequency modeling at small ungauged sites. *J. Hydrol.*, **345**, doi:10.1016/j.jhydrol.2007.07.011.
- Falvey, M., and R. D. Garreaud, 2005: Moisture variability over the South American altiplano during the South America Low Level Jet Experiment (SALLJEX) observing season. *J. Geophys. Res.*, **110**, D22105, doi:10.1029/2005JD006152.
- Goel, N. K., R. S. Kurothe, B. S. Mathur, and R. M. Vogel, 2000: A derived flood frequency distribution for correlated rainfall intensity and duration. *J. Hydrol.*, **228**, 56–67.
- Hall, T. J., and T. H. Vonder Haar, 1999: The diurnal cycle of west Pacific deep convection and its relation to the spatial and temporal variation of tropical MCSs. *J. Atmos. Sci.*, **56**, 3401–3415.
- Houze, R. A., Jr., and D. D. Churchill, 1987: Mesoscale organization and cloud microphysics in a Bay of Bengal depression. *J. Atmos. Sci.*, **44**, 1845–1868.
- , D. C. Wilton, and B. F. Smull, 2007: Monsoon convection in the Himalayan region as seen by the TRMM precipitation radar. *Quart. J. Roy. Meteor. Soc.*, **133**, 1389–1411, doi:10.1002/qj.106.
- Huffman, G., R. Adler, M. Morrissey, D. Bolvin, S. Curtis, R. Joyce, B. McGavock, and J. Susskind, 2001: Global precipitation at one-degree daily resolution from multisatellite observations. *J. Hydrometeorol.*, **2**, 36–50.
- , and Coauthors, 2007: The TRMM Multisatellite Precipitation Analysis (TMPA): Quasi-global, multiyear, combined-sensor precipitation estimates at fine scales. *J. Hydrometeorol.*, **8**, 38–55.
- Iguchi, T., T. Kozu, R. Meneghini, J. Awaka, and K. Okamoto, 2000: Rain-profiling algorithm for the TRMM precipitation radar. *J. Appl. Meteor.*, **39**, 2038–2052.
- Jiang, H., and E. J. Zipser, 2010: Contribution of tropical cyclones to the global precipitation from eight seasons of TRMM data: Regional, seasonal, and interannual variations. *J. Climate*, **23**, 1526–1543.
- Joyce, R. J., J. E. Janowiak, P. A. Arkin, and P. Xie, 2004: CMORPH: A method that produces global precipitation estimates from passive microwave and infrared data at high spatial and temporal resolution. *J. Hydrometeorol.*, **5**, 487–503.
- Kummerow, C., W. Barnes, T. Kozu, J. Shiue, and J. Simpson, 1998: The Tropical Rainfall Measuring Mission (TRMM) sensor package. *J. Atmos. Oceanic Technol.*, **15**, 809–817.
- , and Coauthors, 2001: The evolution of the Goddard Profiling Algorithm (GPROF) for rainfall estimation from passive microwave sensors. *J. Appl. Meteor.*, **40**, 1801–1820.
- Liu, C., and E. J. Zipser, 2005: Global distribution of convection penetrating the tropical tropopause. *J. Geophys. Res.*, **110**, D23104, doi:10.1029/2005JD006063.
- , and —, 2008: Diurnal cycles of precipitation, clouds, and lightning in the tropics from 9 years of TRMM observations. *Geophys. Res. Lett.*, **35**, L04819, doi:10.1029/2007GL032437.
- , and —, 2009: “Warm rain” in the tropics: Seasonal and regional distribution based on 9 years of TRMM data. *J. Climate*, **22**, 767–779.
- , —, and S. W. Nesbitt, 2007: Global distribution of tropical deep convection: Different perspectives using infrared and radar as the primary data source. *J. Climate*, **20**, 489–503.
- , —, D. J. Cecil, S. W. Nesbitt, and S. Sherwood, 2008: A cloud and precipitation feature database from 9 years of TRMM observations. *J. Appl. Meteor. Climatol.*, **47**, 2712–2728.
- , E. Williams, E. J. Zipser, and G. Burns, 2010: On the diurnal variations of global thunderstorms and the global atmospheric electrical circuit. *J. Atmos. Sci.*, **67**, 309–323.
- Mohr, K. I., and E. J. Zipser, 1996: Mesoscale convective systems defined by their 85-GHz ice scattering signature: Size and intensity comparison over tropical oceans and continents. *Mon. Wea. Rev.*, **124**, 2417–2437.
- , J. S. Famiglietti, and E. J. Zipser, 1999: The contribution to tropical rainfall with respect to convective system type, size, and intensity estimated from the 85-GHz ice-scattering signature. *J. Appl. Meteor.*, **38**, 596–606.
- Nesbitt, S. W., and E. J. Zipser, 2003: The diurnal cycle of rainfall and convective intensity according to three years of TRMM measurements. *J. Climate*, **16**, 1456–1475.
- , —, and D. J. Cecil, 2000: A census of precipitation features in the tropics using TRMM: Radar, ice scattering, and lightning observations. *J. Climate*, **13**, 4087–4106.
- , —, and C. D. Kummerow, 2004: An examination of version 5 rainfall estimates from the TRMM microwave imager, precipitation radar, and rain gauges on global, regional, and storm scales. *J. Appl. Meteor.*, **43**, 1016–1036.
- , R. Cifelli, and S. A. Rutledge, 2006: Storm morphology and rainfall characteristics of TRMM precipitation features. *Mon. Wea. Rev.*, **134**, 2702–2721.
- Orville, R. E., and R. W. Henderson, 1986: Global distribution of midnight lightning: September 1977 to August 1978. *Mon. Wea. Rev.*, **114**, 2640–2653.
- Salio, P., M. Nicolini, and E. J. Zipser, 2007: Mesoscale convective systems over southeastern South America and their relationship with the South America Low-Level Jet. *Mon. Wea. Rev.*, **135**, 1290–1309.
- Schumacher, C., and R. A. Houze Jr., 2003: The TRMM precipitation radar’s view of shallow, isolated rain. *J. Appl. Meteor.*, **42**, 1519–1524.
- Seo, E., B. Sohn, and G. Liu, 2007: How TRMM precipitation radar and microwave imager retrieved rain rates differ. *Geophys. Res. Lett.*, **34**, L24803, doi:10.1029/2007GL032331.
- Skok, G., J. Tribbia, J. Rakovec, and B. Brown, 2009: Object-based analysis of satellite-derived precipitation systems over the low- and midlatitude Pacific Ocean. *Mon. Wea. Rev.*, **137**, 3196–3218.
- Spencer, R. W., H. M. Goodman, and R. E. Hood, 1989: Precipitation retrieval over land and ocean with SSM/I: Identification and characteristics of the scattering signal. *J. Atmos. Oceanic Technol.*, **6**, 254–273.
- Toracinta, E. R., and E. J. Zipser, 2001: Lightning and SSM/I ice scattering MCSs in the global tropics. *J. Appl. Meteor.*, **40**, 983–1002.
- , —, D. J. Cecil, and S. W. Nesbitt, 2002: Radar, passive microwave, and lightning characteristics of precipitating systems in the tropics. *Mon. Wea. Rev.*, **130**, 802–824.

- Velasco, I., and J. M. Fritsch, 1987: Mesoscale convective complexes in the Americas. *J. Geophys. Res.*, **92**, 9591–9613.
- Wang, N.-Y., C. Liu, R. Ferraro, D. Wolff, E. J. Zipser, and C. Kummerow, 2009: The TRMM 2A12 land precipitation product—Status and future plans. *J. Meteor. Soc. Japan*, **87A**, 237–253.
- Wilheit, T., 1986: Some comments on passive microwave measurement of rain. *Bull. Amer. Meteor. Soc.*, **67**, 1226–1232.
- Xu, W., E. J. Zipser, and C. Liu, 2009: Rainfall characteristics and convective properties of mei-yu precipitation systems over south China and Taiwan. Part I: TRMM observations. *Mon. Wea. Rev.*, **137**, 4261–4275.
- Yamamoto, M. K., F. A. Furuzawa, A. Higuchi, and K. Nakamura, 2008: Comparison of diurnal variations in precipitation systems observed by TRMM PR, TMI, and VIRS. *J. Climate*, **21**, 4011–4028.
- Yang, G.-Y., and J. Slingo, 2001: The diurnal cycle in the tropics. *Mon. Wea. Rev.*, **129**, 784–801.
- Zipser, E., D. Cecil, C. Liu, S. W. Nesbitt, and D. Yorty, 2006: Where are the most intense thunderstorms on Earth? *Bull. Amer. Meteor. Soc.*, **87**, 1057–1071.